Ahuir-Torres, JI, Chen, X, Akar, Y, Bingham, PA, Jackson, FF, Li, H, Mason, L, Mishra, R, Walker, DD and Yu, G

Influence of the grain chemical composition on the fused silica polishing at atomic scale using molecular dynamic simulations

Ceramics International 51 (2025) 9278–9291

Contents lists available at ScienceDirect

Ceramics International

journal homepage: www.elsevier.com/locate/ceramint

Influence of the grain chemical composition on the fused silica polishing at atomic scale using molecular dynamic simulations

Juan I. Ahuir-Torres [a,*], Xun Chen [a,**], Yasemin Akar [b], Paul A. Bingham [c], Frankie F. Jackson [d], Hongyu Li [f], Luke Mason [e], Rakesh Mishra [d], David D. Walker [f], Guoyu Yu [f]

[a] General Engineering Research Institute, Faculty of Engineering and Technology, Liverpool John Moores University, GERI Building, 3 Byrom Street, Liverpool, Merseyside, L3 3AF, United Kingdom
[b] Faculty of Engineering and Physical Sciences, School of Mechanical Engineering, University of Leeds, Woodhouse, Leeds, LS2 9JT, United Kingdom
[c] College of Business, Technology and Engineering, Sheffield Hallam University, City Campus, Howard Street, Sheffield, South Yorkshire, S1 1WB, United Kingdom
[d] Department of Engineering and Technology, School of Computing and Engineering, University of Huddersfield, Huddersfield, West Yorkshire, HD1 3DH, United Kingdom
[e] SciTech Daresbury National Science & Innovation Campus, University of Huddersfield Laboratory for Ultra Precision Surface, G6 TechSpace One Keckwick Lane, Daresbury, Merseyside, WA4 4AB, United Kingdom
[f] Scientific Computing Department, Science and Technology Facilities Council, North Star Avenue, Swindon, Wiltshire, SN2 1SZ, United Kingdom

ARTICLE INFO

Handling editor: P. Vincenzini

Keywords:
Optical glass material polishing
Grain chemical composition
Fused silica
Molecular dynamic
Tersoff
Material removal rate

ABSTRACT

The optical glass materials are employed in various industries due to its desirable optical properties. These materials nevertheless require an ultra-smooth surface (Ra <1 nm average roughness) for correctly working. The understanding of the polishing process is essential to get the ultra-smooth surface. The polishing process begins at atomic scale, hindering its study in real time using experimental testing. Molecular dynamic (MD) simulation is powerful tool to assess this process at atom scale in real time. Although the influence of various polishing conditions on polished surface features has been evaluated in the literature, the grain chemical composition influence has not been studied yet. In the present paper, this condition influence on optical glass material polishing at atom scale was assessed using MD simulation. Fused silica was employed as optical glass test pieces, and the abrasive grains used were α-quartz, diamond and α-alumina. Force on the grain was from 0.5 pN to 16.0 pN and cut velocity was 20 m/s. Tersoff potential function method was used to represent the covalent bonds of the materials. The results showed simulations at ≥ 2.0 pN were unstable during polishing due to the mechanical failure. Grain sliding also produced a new microstructure in the glass via the dislocation and deformation of the chemical bonds. The material removal rate (MRR) furthermore was directly proportional to the grain force and the hardness of the grain. The increment in the grain force increased the friction force. Grain chemical composition moreover influenced on the polishing phenomena.

1. Introduction

Optical glass materials are an essential element in various industries as, laser, telecommunications, astrophysics, aerospace, automotive and optics. The fused silica is the base material to produce other optical glass material and one of the main optical glasses [1–3]. The optical glass requires an extra smooth surface to avoid optical aberrations. This can be achieved through grinding, lapping and polishing processes [4–6]. Depending on the conditions (e.g., force on the grain, sliding velocity and abrasive type), the polishing processes can result in both surface and internal damages to the optical glass material [4,7–9]. These conditions also have a strong influence on the material removal rate (MRR), being one of key factor of the polishing quality [9]. Thus, the study of the polishing parameter influence on the surface quality is essential to achieve the conditions to generate the optical glass material with the best characteristics. The chemical composition of the abrasive powder is a crucial factor in optical glass polishing. This characteristic defines on only the mechanical properties of the grain but also the chemical interaction between fused silica and the abrasive powder, both of which

* Corresponding author.
** Corresponding author.
E-mail addresses: j.i.ahuirtorres@ljmu.ac.uk (J.I. Ahuir-Torres), x.chen@ljmu.ac.uk (X. Chen).

https://doi.org/10.1016/j.ceramint.2024.12.363
Received 7 November 2024; Received in revised form 12 December 2024; Accepted 20 December 2024
Available online 27 December 2024

Nomenclature

α-Al_2O_3	α-Alumina
Al	Aluminium
θ_{ijk}	Angle between bonds ij and ik
$g_{ik}(\theta_{ijk})$	Angular function represented
A_A	Arch area of the grain semi-sphere part
f_A	Attractive function
b_{ij}	Bond formation energy
R	Cut off function
V_C	Cut velocity
D_o	Dimer bond energy
ζ	Effective coordination number
m	Empirical factor
h	Energetically optimum angle cosine
β	Fitting parameters
S	Fitting parameters
a-SiO_2	Fused Silica
F_G	Grain pressure force
r_G	Grain radius
HPC	Hexagonal Close-Packed
r_{ij}	Interatomic distance
λ_3	Inverse distance of the nearest neighbour
LAMMPS	Large-scale Atomic/Molecular Massively Parallel Simulator
MRR	Material Removal Rate
b_{ij}	Many-body bond-order parameter
MD	Molecular Dynamic
n	Number of the neighbour atom
O	Oxygen
f_A	Pairwise attractive
f_R	Pairwise repulsive
θ	Penetration angle
D_p	Penetration depth
R_G	Penetration depth rate
A_p	Pylon area of the grain cylindrical part
α-SiO_2	α-Quartz
D	Radius of region
$f_R(r_{ij})$	Repulsion function
d	Sharpness of the dependence on angle
Si	Silicon
ΔX_p	Sliding distance after the penetration depth is larger than the grain radius
f_c	Spherical cut-off function
c	Strength of the angular effect
σ_{XX}	Stress in X direction
σ_{XY}	Stress in X-Y direction
σ_{XZ}	Stress in X-Z direction
σ_{YY}	Stress in Y direction
σ_{YZ}	Stress in Y-Z direction
σ_{ZZ}	Stress in Z direction
t_p	Time after $D_p = r_G$
E_{Total}	Total energy of the system
t	Total sliding time
σ	Von Mises stress

influence on the polishing process mechanism. The polishing process starts with the interaction between grain and optical glass material at atomic scale. The evaluation of this process at atom scale in real time is currently impossible using experimental testing because of the intrinsic difficulties [10–13].

Molecular dynamic (MD) simulation can be an optical method to conduct this type of studies [10–13]. MD simulation is a semi-empirical method that permits to determine the trajectory of the elements with numerically Newton's equations of motion for a system of the interacting particles. Forces, kinetic and potential energy of the particles are estimated using simulation element force fields [14,15], which contribute to analyses the interactions between materials at nanoscale. These interactions encompassed the physical chemistry phenomena are integrated to the mechanical processes. While other simulation methods (e.g., finite and discrete elements) are effective to simulate the mechanical and physical behaviour of the material across processes, they can only approximate the chemical interactions. The Monte Carlos method, though capable of simulating similar process, produces physical and chemical unrealistic phenomena due to its inherent randomness [16,17]. For these reasons, MD has been utilised to simulate the machining processes (e.g., cutting, lapping, grinding, scratching and polishing) of several materials at various conditions.

The research group of Han [9] studied the silicon polishing with diamond at nanometre scale using MD with Tersoff and Morse potential function fields. Their findings revealed that the high hydrostatic pressure generated during the polishing process induced microstructural changes in silicon, leading the crack formation. Later, Tian et al. [18] explored the penetration depth influence on the 4H-SiC and 6H-SiC polishing process using MD simulator code with Tersoff potential function field. Their study identified amorphous transformation and the dislocations as the primary mechanism governing MRR. Wu et al. [19] conducted simulations of 6H-SiC polishing using MD-LAMMPS with Tersoff potential function field. Their finding revealed that the material plastic deformation occurred due to amorphization and dislocation activity. The double polishing tracks at short length between grains leads the creation of new crystalline structure creation in the zone between scratching. This phenomenon is attributed high temperature and stress in this region. Gou research group [20] investigated the fused silica polishing with diamond at atom scale through MD employed Tersoff as potential function field. Their study identified that the densification of the fused silica resulted in the embrittlement of the material, which was determined as primary mechanism for material removal. Luo et al. [21] conducted an investigation on the 6H-SiC polishing with diamond grain using MD-LAMMPS with Tersoff and Lennard-Jones as the potential function fields. Their findings showed that wear debris on scratch exhibited microstructural heterogeneity. The material removal rate, as well as normal and friction force were found directly proportional to the cut depth. Notably, the cracks formation were found at 8 nm penetration depth or larger.

Although the physical polishing condition influence on the material removal and surface quality at atom scale has widely been studied in the literature using MD, the effect of the abrasive powder chemical composition has been rarely evaluated. The chemical composition of the abrasive particle plays a crucial role in the polishing process, as it not only defines the mechanical properties of the abrasive powder but it also determines the chemical interactions between the optical glasses with abrasive particles. These interactions can significantly influence on the polishing performance and surface quality. However, many previous studies have overlooked this factor in the modelling of the polishing process, limiting its full understanding of the process. Therefore, the impact of the abrasive powder chemical composition on the optical glass polishing represents a significant gab in the current modelling of this process.

For these reasons, this paper investigated grain chemical composition and force on the grain influence on the fused silica polishing process. α-quartz, diamond and α-alumina were the abrasive powder used as grain, which are most common abrasive powder employed in the optical glass polishing. The comparison of the simulation results

(mechanical, thermodynamic and physical) for the various types of abrasive powder type, enabled the identification of the effect of chemical composition on the optical glass polishing, which is a factor ignored in previous studies. To achieve this aim, the study established the following objectives.

(i) Determination of the material removal mechanism corresponding to each force and grain type.
(ii) Evaluation and study of the possible damages generated during the polishing according to the polishing conditions.
(iii) Analysis of the tribological processes during optical glass polishing force and grain type.
(iv) Modelling the material removal rate in function to applied force for each grain type.

Tersoff potential function field was employed as potential field in this study to simulate a system formed of materials with covalent bonds. Although other potential functions (e.g., Reaxff) can simulate the chemical reactions, Tersoff is an adequate function to simulate the covalent material [13,22] in acceptable computational time [23].

2. Methodology

2.1. Methods and general conditions of the system

In this investigation of polishing process, the large-scale atomic/molecular massively parallel simulator (LAMMPS) [24] was utilised for carrying out the MD simulations of interactions between abrasive grit and fused silica glass. In this paper, all simulations were carried out with real units, full atom style, in 3 dimensions with f p f boundary and, at 3.0 bin of neighbour (defined in LAMMPS [12]). The real units and full atom style were chosen to enable to add the original charges of the atoms, which were assigned appropriately to ensure the precise simulating of the chemical interactions between elements. The f p f boundary of the overall simulation box indicates that the simulation space boundary in X and Z directions are fixed (using f letter), while the boundary in Y direction is periodic (with p letter), meaning the atoms can interact with the sides of the box. The non-interactions of the opposite side atoms (f letter) for fixed boundary prevents the superposition of the interference from the boundary effect [25]. The radius of the interaction between atoms is function of the potential force field plus 0.3 nm according to 3.0 bin and real unit. An open visualisation tool Ovito Basic software was used to visualise the simulation results. The software also enabled to visualise and quantify the material removal, penetration depth, dislocations, elastic and plastic deformation. The maximum Von Mises stresses were moreover measured with Ovito [26].

2.2. Simulated materials and model setup

The system of the simulation was constructed with a workpiece and a polishing tool, as shown in Fig. 1(a). The grain was placed in the right side of the workpiece block in X axis, at the middle of the Y axis and at 5 nm from the top of workpiece in Z axis. The workpiece size was 55.8 nm × 20.3 nm X 12.1 nm (X, Y, Z) and the atom number of the workpiece was 1010988. The optical glass material of the workpiece was fused silica (α-SiO_2), which comprised of silicon cations (+4 valence) and oxygen anion (−2 valence) [27]. The fused silica was generated using an annealing or quenching process simulation of the α-quartz. This annealing was simulated via subsequent two steps: heating step and then cooling step. The heating of the α-quartz at 4000 K was conducted using velocity create command of Gaussian distribution (e.g., velocity Region create 4000.0 4928459 dist gaussian). The cooling process was carried out for 40 ps with −100 K/ps of the cooling speed with canonical ensemble (NVT) (e.g., fix ID Region nvt temp 4000 300 10) for the atom trajectory and velocity [28,29]. The optical glass material formed of three layers to stabilise the simulation, which were specified as following.

- Boundary layer was placed in the bottom and X axis the left side of the workpiece with a thickness of 1.0 nm. The boundary layer was set to be a constant position for all simulation time (NVE/noforce command). This layer represents the section of the optical glass material outside the polished zone and keeps the microstructure of the sample.

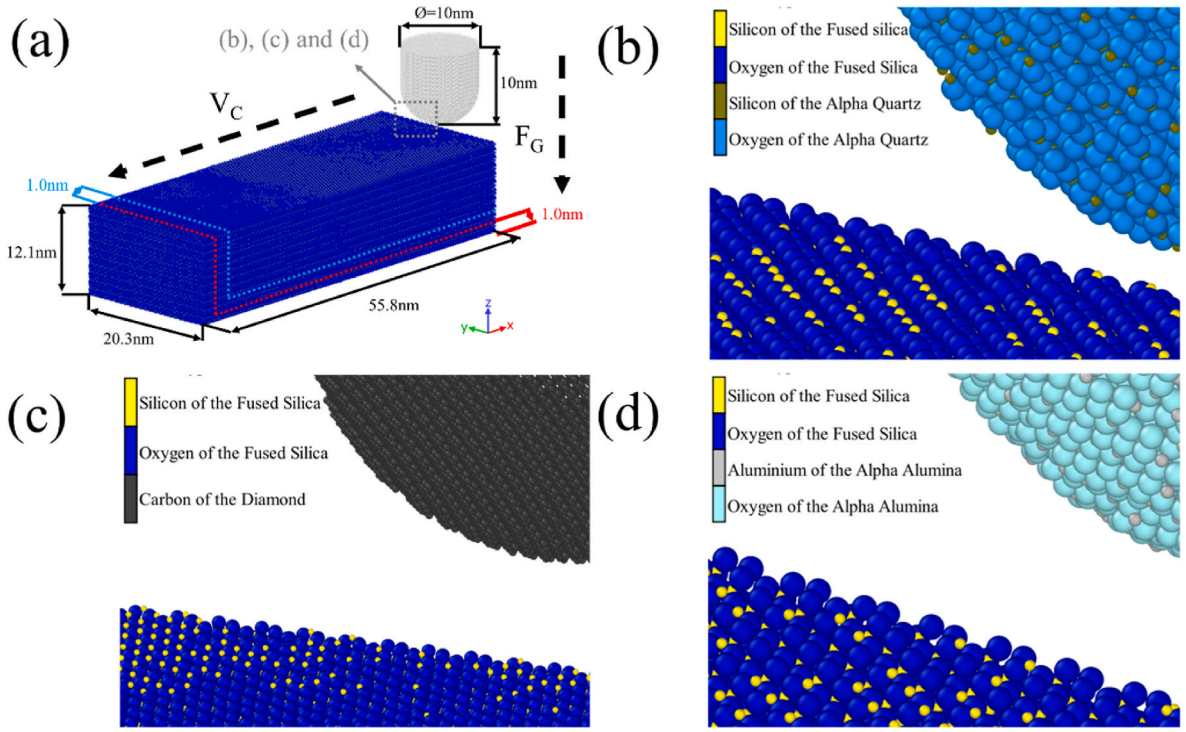

Fig. 1. MD system of the optical glass material (fused silica) polishing with polishing tool (a), being α-quartz (b), diamond (c) and α-alumina (d).

- Thermostatic layer was localised on top or right to the boundary layer with a thickness of 1.0 nm. This layer was used to simulate the diffusion heat into the bulk material by means of thermal conductivity. This diffusion was achieved with Berendsen thermostat for the temperature simulation and NVT for the atom trajectory and velocity modelling.
- Newtonian layer was the last layer that was the rest of the workpiece, which acts as the polishing zone where the abrasive grain interacted with the optical glass material. The velocity and trajectory of the layer atoms was simulated using microcanonical ensemble (NVE).

It is important note to the system of three layer is commonly reported in the literature [9,13,20,30–33].

The abrasive grain on the polishing tool formed of a semi-sphere of 5 nm radius, joined a cylinder with 5 nm height on the bottom as shown in Fig. 1(a). The grains was a hollow rigid body of 1 nm thickness to reduce the computing time [13]. The grain was modelled as a rigid body due to the significantly higher hardness of the α-quartz, diamond and α-alumina compared to fused silica [12,13,34]. The grains were α-quartz (Fig. 1(b)), diamond (Fig. 1(c)) and α-alumina (Fig. 1(d)) grains. The α-quartz grain (α-SiO_2) was formed of silicon cation with +4 valence (Si^{+4}) and oxygen anion of −2 valence (O^{-2}), containing 24936 atoms. The crystalline structure of α-SiO_2 was similar hexagonal closed packaged (HCP) [35]. Diamond grain was consisted of carbon atoms with partial charge of 0, forming of 56279 atoms. The crystalline structure of diamond was similar to face centred cubic [36]. The aluminium cation with +3 valence (Al+3) and the oxygen anion with −2 valence (O^{-2}) formed α-alumina. The grain was consisted of 37895 atoms that were placed according to the crystalline structure of the α-alumina (HCP) [37].

The force fields of the atoms were simulated using Tersoff potential function method of three bodies. This method provides a good realistic representation of the covalent bonds various bodies, allowing to get realistic results [13,18]. Dissimilar Tersoff potential functions were employed according to the grain type material. For the simulations of the a-SiO_2 polishing with α-SiO_2, the SiO Tersoff potential function from the literature [38] was used. In the case of the polishing processes simulated with diamond and α-Al_2O_3 grains, Tersoff potential functions were designed by the researchers and were named as SiCO and SiOAl, respectively. The development of new potential functions involved the combination two exiting Tersoff potential function. SiC [39] and SiO [38] potentials were combined for SiCO, while SiO [38] and AlO [40] were integrated for SiOAl. This method aligned with the approach previously employed in the study of Brugnoli et al. [41].

2.3. Tersoff interatomic potential

Tersoff interatomic potential is a powerful computational tool for material interactions based on the principles of quantum chemistry and mechanics. Tersoff force field permits to simulate the covalent atomic interactions via the representation of the attractive and repulsive forces between atoms. The total energy of the system (E_{Total}) is represented using equation (1) [13,31,38,40,42,43].

$$E_{Total} = \frac{1}{2}\sum_{i}\sum_{j\neq i} f_c(r_{ij})\left[f_R(r_{ij}) - b_{ij} f_A(r_{ij})\right] \quad (1)$$

Where, f_c is the spherical cut-off function, f_R is pairwise repulsive, f_A is pairwise attractive, r_{ij} is the interatomic distance and b_{ij} is the many-body bond-order parameter. The spherical function (f_c) was restricted to the next neighbour sphere by cut off function (R) as can be seen in equation (2) [18,20,44].

$$f_c(r_{ij}) = \begin{cases} 1 & r_{ij} < R - D \\ \frac{1}{2} - \frac{1}{2}\sin\left[\frac{\pi x (r_{ij} - R)}{2 * D}\right] & R - D \le r_{ij} \le R + D \\ 0 & r_{ij} > R + D \end{cases} \quad (2)$$

Being, D the radius of region. The repulsion function ($f_R(r_{ij})$) is determined by chemical bonds parameters as can be found in equation (3) [38,43].

$$f_R = \left[\frac{D_o}{S-1}\right] x exp\left[-\beta x\sqrt{2xS}\, x(r_{ij})\right] \quad (3)$$

Where, D_o is dimer bond energy, β and S are fitting parameters. b_{ij} renders the bond formation energy, which is influenced by atom neighbour and, whose function is represented by equation (4) [20,38,40].

$$b_{ij} = \left(1 + \beta_i^n x \zeta_{ij}^n\right)^{\frac{-1}{2n}} \quad (4)$$

Being, n the number of the neighbour atom and ζ the effective coordination number, whose function can be seen in equation (5) [38,40,42].

$$\zeta_{ij} = \sum_{k\neq i,j} f_c(r_{ik}) x g_{ik}(\theta_{ijk}) x exp\left(\lambda_3^m x (r_{ij} - r_{ik})^m\right) \quad (5)$$

Where, λ_3 is the inverse distance of the nearest neighbour, m is the empirical factor and $g_{ik}(\theta_{ijk})$ is angular function represented by equation (6) [20,40,43].

$$g_{ik}(\theta_{ijk}) = \gamma_{ijk} x \left(1 + \frac{c_{ik}^2}{d_{ik}^2} - \frac{c_{ik}^2}{\left[d_{ik}^2 + (h_{ik} - \cos(\theta_{ijk})^2\right]}\right) \quad (6)$$

Being, θ_{ijk} the angle between bonds ij and ik, h energetically optimum angle cosine, c the strength of the angular effect and d the sharpness of the dependence on angle.

The attractive function (f_A) is furthermore determined by the chemical bond features as can be identified in equation (7) [38,40,43].

$$f_A(r_{ij}) = \left[\frac{SxD_o}{S-1}\right] x exp\left[-\beta x\sqrt{\frac{2}{s}}\, x(r_{ij})\right] \quad (7)$$

Tersoff potential functions utilised these equations to calculate the covalent bonds feature with the parameters of Table 1.

2.4. Process conditions for polishing simulation

The polishing simulations was consisted of three steps: initialisation, downward contact and polishing part (Fig. 2).

The assembled atom system was stabilised for the first 1605 ps in the initialisation stage of the simulation (Fig. 3). The system deemed stable

Table 1
Parameters in Tersoff potential function for silicon (Si), oxygen (O), carbon (C) and aluminium (Al) employed to simulate the chemical interactions.

Parameters	Si [38,39,45]	O [38,45]	C [43,45]	Al [40]
D_o (eV)	2465.3919	1664.0615	114.8282	1.5000
S	0.2574	0.1162	0.2488	2.7876
β (A^{-1})	0.8788	0.8304	0.7801	1.0949
R (A)	2.5000	1.7000	1.8000	2.7000
D (A)	2.6500	1.8500	1.9500	0.1000
n	0.7873	1.0497	0.7275	6.0865
λ_3 (A^{-1})	0.0000	0.0000	0.0000	1.5000
m	3.0000	3.0000	3.0000	3.0000
γ	1.0000	1.0000	1.0000	0.3168
c	100390.0000	6492.1000	38049.0000	0.0748
d	16.2170	4.1113	4.3840	19.5691
h	−0.6593	−0.8456	−0.5706	−0.6593

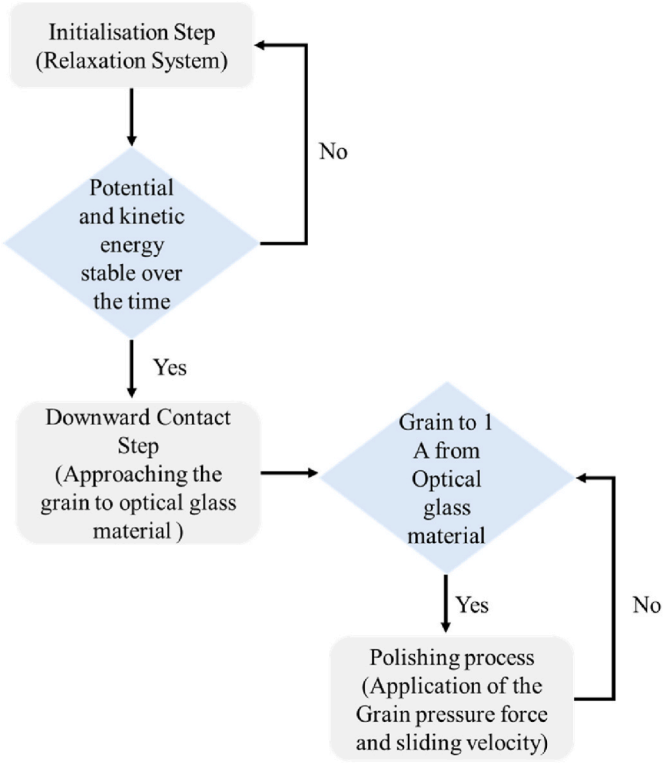

Fig. 2. Flowchart of the simulations.

when both the potential (Fig. 3(a)) and kinetic energy (Fig. 3(b)) remained constant over time.

After initialisation step, the grain moved down to 1 Å above the optical glass surface. From this point in the polishing simulation, the force (F_G) was applied on the grain in -Z direction, and the grain was moving horizontally with cut velocity ($V_C = -20$ m/s [9,32,33]) along X axis. The simulation system setup can be observed in Fig. 1(a). Selected F_G in simulation were 0.5 pN, 1.0 pN, 2.0 pN, 4.0 pN, 8.0 pN and 16.0 pN.

3. Results and discussion

3.1. Thermodynamic phenomena

The evolution of the simulated system stability over the time was assessed via the potential energy, which can be seen in Fig. 4 The potential energy of the system represents the cohesion of the system atoms for each other [45,46].

All simulations demonstrated an increase in the potential energy during the initial 200 ps, attributed to the initial pressure exerted by the grain on fused silica, which compressed the material. This compression process led to a reduction in the chemical bonds within the fused silica. The potential energy for the Tersoff function potential field is proportional to the bond length [38,40,43,47].

After its initial increase, the potential energy remained constant certain period, which was dependent grain pressure force and gain type. The time duration was reduced with the increase in grain pressure force due to the corresponding rise in stress [3,18,45]. The type of the grain exhibited an unclear pattern influence on the time, which will be discussed in detail in subsequent sections. Subsequently, the potential began to fluctuate over time. Prior to the grain penetrated into the optical glass materials, the grain sliding induces a microstructural deformation on the optical glass surface. The deformation is attributed to changes in atom positions, which altered the chemical bond length. The redistribution of the atom position was the responsible for the potential fluctuations observed. The decreasing of the potential energy is attributed to the enlargement of the bond lengths, caused by the combination of grain pressure and sliding on the fused silica.

Once the grain passed, the fused silica atoms recover the bond length, resulting in an increase of the potential energy [19,39]. Over extended period, a reduction of the potential energy over time was observed, attributed to the grain has penetrated into fused silica. This period also depended on the grain type and normal force level with similar behaviour to the previous case. The grain penetration induces the displacement of the atoms at over long distances, leading diminishes the potential energy of the system. The new microstructure formed in the fused silica due to the grain penetration further reduces the potential energy, which is attributed to the less stability of the new microstructure [46].

The slope of the potential energy reduction with time changes in specific point for all cases with loading force is $\geq$ 2.0 pN, which is attributed to the chip formation. The breaking of the chemical bonds during the chip formation results in decrease the potential energy, as it is directly proportional to number of the chemical bonds [46]. It is important to note that the system became unstable when the potential energy reached specific values, which was defined by the grain type. This phenomenon was attributed to varying chemical composition of the grain, which will be discussed in detail in subsequent section. The point at which the simulation system became unstable is referenced to as the unstable system point, which was defined by the normal force on the grain. This could be attributed to the material melting or mechanical failures such as crack generation or pulverisation, which will be discussed later.

The values of the potential energy were different according to the type of grain, where the lowest value was found for α-quartz (Fig. 4(a)) and the highest was for diamond (Fig. 4(c)). Obviously, this indicates that the diamond grain is the most stable while the α-quartz is the less stable. This phenomenon is attributed to the higher number of the bond and bond energy for the diamond molecules (e.g., 4 × 868 = 3472 kJ/

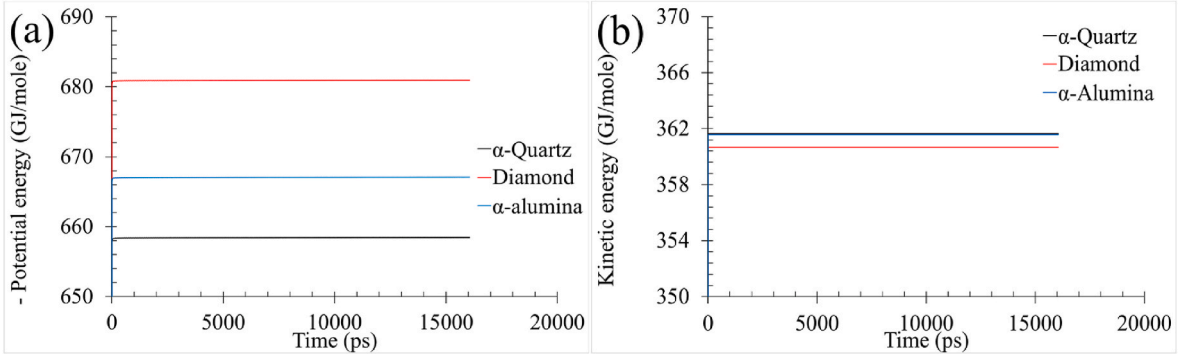

Fig. 3. Temporal evolution of the potential (a) and kinetic (b) energy of the polishing systems.

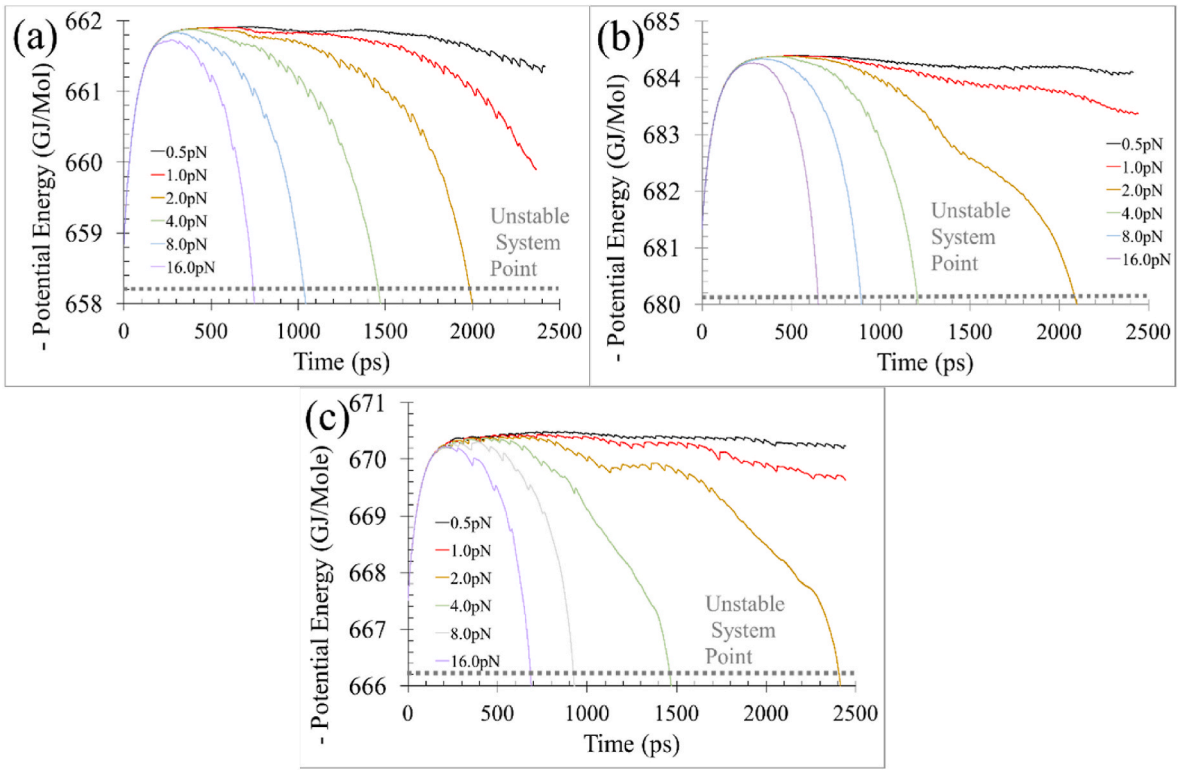

Fig. 4. Evolution of the system potential energy over time according to grain force for α-quartz (a), diamond (b) and α-alumina (c) grain used to polish the fused silica.

mol C-C-C-C [48]; 2 × 798 = 1596 kJ/mol O-Si-O [49]; 4 × 773 = 3092 kJ/mol O-Al-O-Al-O [49]). The potential energy is proportional to the bond number and energy [13,31,38,40,42,43]. Notably, the potential energy is indicative of the material thermodynamic stability, which is governed by the chemical interaction between its constituent atoms. Consequently, the potential energy can vary in rigid bodies with different chemical composition.

The temperature is another significant parameter in determining the

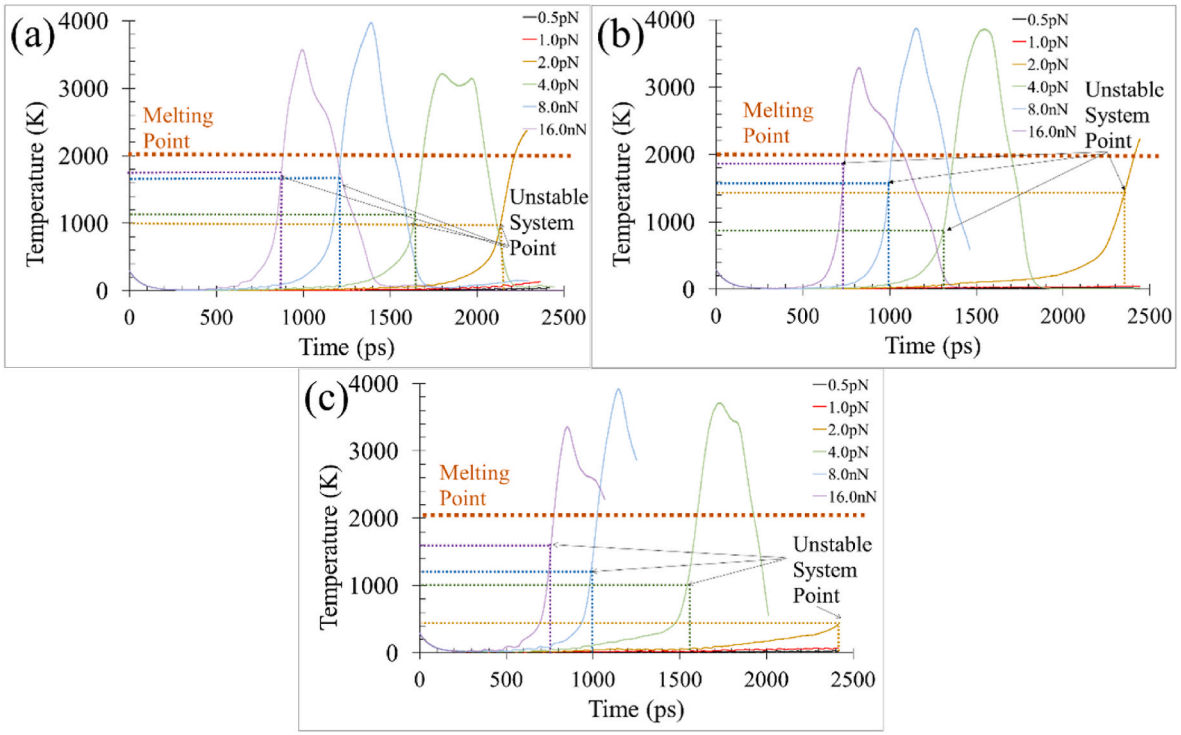

Fig. 5. Evolution of the optical glass material temperature over time according to grain force for α-quartz (a), diamond (b) and α-alumina (c) grain used to polish the fused silica.

stability of the system during the polishing. The temporal evolution in relation to the grain pressure force and grain type can be seen in Fig. 5. Three different behaviours were observed in the temporal temperature evolution of the simulations, which was classified depending on the grain pressure force. The first behaviour occurred at the grain pressure force < 2.0 pN, the second at 2.0 pN and, the last at > 2.0 pN for all grain types.

The first behaviour was featured by an initial quick reduction in the temperature with time due to the high thermal energy absorption from fused silica by the thermostatic layer. Due to the absence of the external force at the initial move on the fused silica atoms, the temperature of the optical glass material reaches the 0 K within ≤ 200 ps. This phenomenon is because the temperature is a representation of the atom movement [45]. The low normal force and friction energy provokes a scarce heat in the material, resulting in the low temperature [50]. At 200 ps, the fused silica reached the 0 K and subsequently, the temperature was slowly increased with time until the end of the simulation. A part of the grain kinetic energy is converted to heat in optical glass material during the grain sliding on surface due to the friction [50,51].

Second behaviour was similar to the previous but with a rapid temperature increase at the end of the simulation, where a significant material deformation became evidence. The displacement of the atoms during the material removal generates the breaking of the chemical bonds, which is an exothermic process. The heat generated in this process is directly proportional to the number of the broken chemical bond. Consequently, the increase in the removed material amount over time increases the temperature of the optical glass materials exponentially [52,53].

The last temporal evaluation type behaviour was similar to the previous types; but it presented differences in the last stage. The fused silica temperature increased up to specific point, and then rapidly dropped down, potentially to 0 K. The continuous breaking of the chemical bonds during the simulation creates permanent broken smaller glass particles, even becoming single molecules of oxide silicon (SiO_2). The molecules have higher movement freedom compared with the molecules of the bulk material. These molecules can reach fast velocities due to the energy provided by the breaking of the chemical bonds. When molecules escape from the simulated cell, reducing in the number of the elements with high velocity in the cell. Consequently, the temperature of the system is decreased with time at this stage.

The transition time between steps for the temporal temperature varies depending on the grain type, exhibiting an unclear influence pattern. The heat produced during the polishing can be dissipated by the grains via thermal diffusion. Grains possess different thermal diffusivity according to the chemical composition (α-quartz (3.62–7.87 mm^2/s) [54], diamond (185000 mm^2/s) [55] and α-alumina (88–300 mm^2/s) [56]). This dissimilarity between grains type causes the variation of temperature elevation. Dissimilar polishing mechanisms also varies MRR, which can alter the fused silica temperature in different ways. The polishing mechanisms according to the grain type and the grain pressure force on the grain will be discussed in the next section (Section.3.2. Mechanical Phenomena).

The simulations shows that the system became unstable at specific point for the case when normal force ≥ 2.0 pN, as previously commented. The system unstable points were lower than the melting temperature (1986 K [57]) for all the cases. This discards that the cause of the system destabilisation as a thermal process. Thus, the cracks formation or pulverisation of the material (as a mechanical process) can be the causes of this system instability. Therefore, the temperature increase is only a consequence of the system destabilisation.

The system stable time was defined as the time where the system was stable up to the point when the system became unstable. The system stable time varied based on the grain pressure force and grain type (Fig. 6.). The higher grain pressure force on the grain produced shorter stable time. The formation time of the cracks and pulverisation were encouraged by normal force on the grain. The pressure of the grain on

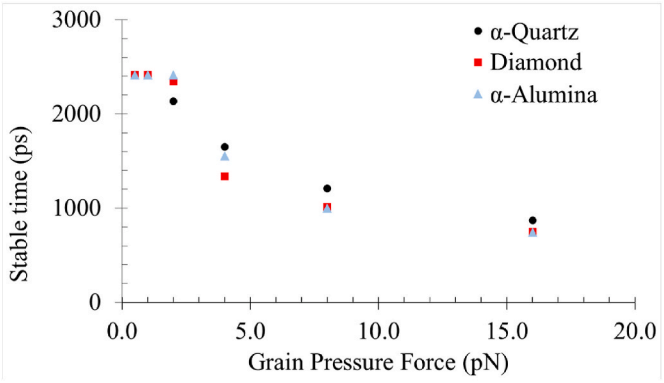

Fig. 6. Graph of the stable time of the system according to the normal force on the grain (grain pressure force) and type of grain.

glass surface is increased with the grain pressure force increase. When the stress produced by grain pressure is higher than the glass strength, the pulverisation and cracking occur [3,18,45]. The reduction of the force on the grain can decrease or eliminate the possibility of these mechanical failures, which was observed for the simulation at ≤ 1.0 pN, where the grain passed all length of the fused silica. It is noteworthy that the system failure due to crack generation was absent at higher grain pressure force in previous studies at wet conditions [53]. This crack formation absence is attributed the presence of the water in the system. The kinetic energy of the fused silica encourages the crack formations by destabilising the chemical bonds. The water absorbs this kinetic energy, thereby reducing the crack generation.

α-alumina and diamond grains had shorter stable time in comparison with α-quartz due to the larger hardness of these grains. The formation of the cracks and pulverisation is prompted to the grain hardness [58]. Diamond, α-alumina and α-quartz possess different hardness, 1600 GPa for diamond and 400 GPa for α-alumina and 100 GPa for α-quartz hardness [59]. The grains with high hardness thus possess more probability to produce mechanical fails on optical glass leading to an unstable process.

3.2. Mechanical Phenomena

Von Mises stress is a significant factor in the failure of the system. Von Mises stress at 1 ps before the system became unstable were illustrated in Fig. 7. From MD simulation, the stresses in the process can be presented by Von Mises stress (σ) that were calculated using equation (8) [60].

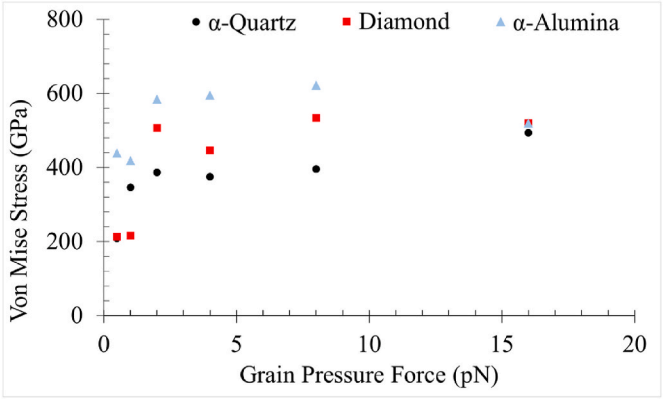

Fig. 7. Graphs of the Von Mises stress influenced by grain type and grain pressure force.

$$\sigma = \sqrt{\sigma_{XX}^2 + \sigma_{YY}^2 + \sigma_{ZZ}^2 - \sigma_{XY} - \sigma_{XZ} - \sigma_{YZ}} \quad (8)$$

Where, σ_{XX} is the stress in X direction, σ_{YY} is the stress in Y direction, σ_{ZZ} is the stress in Z direction, σ_{XY} is the stress in X-Y direction, σ_{XZ} is the stress in X-Z direction and σ_{YZ} is the stress in Y-Z direction. Von Mises stress varied according to the grain pressure force and grain type.

An increase in grain pressure force resulted an increase in the maximum stress for values below 2.0 pN in all case. At higher grain pressure force, the stress remained constant across all grain type. Therefore, under the given polishing condition, 2.0 pN grain pressure force on the grain is high enough to allow the grain to penetrate into the glass. The associated stress represented the glass failure stresses.

α-quart grain simulation had the lowest stresses while the highest stresses were found for the simulation with α-alumina grain. For ≥ 2.0 pN, Von Mises stress were 420 GPa, 500 GPa and, 550 GPa for α-quart, diamond and α-alumina, respectively. The denser grains produces a greater stresses on the optical glass material surface than lighter grains. Thus, the highest stresses were found for α-alumina, having high density (3.9 g/cm^3 [61]) whilst α-quartz was the light material (2.7 g/cm^3 [20]), causing the lowest stresses. The diamond density is 3.5 g/cm^3 [36].

The microstructure and shape of the fused silica underwent changes during the polishing process for all cases (Fig. 8). The moving grain applied a pressure on the optical glass producing stresses on the chemical bonds of the materials, modifying the bond features (e.g. length and position). The chemical bonds undergo deformation when the applied stress excesses the chemical bond resistances. These deformations can result in either an increment or reduction in the bond length, depending on the direction of the stress. The position of the chemical bonds without length modification is also altered due to combination of the applied stress in different directions. Once the stress ceases, the chemical bonds retain their new position because the material atoms attain a new stable state. This process is often called as dislocation [11,18,31–33,45]. This new microstructure was seen in all trajectories of the sliding grain (Fig. 8 (a–f)) and remained after the grain sliding. Such a remained deformation is regarded as plastic deformation [32]. In this zone, some deformation of optical glass materials size can recovered as an elastic recovery process [19,39]. Fig. 9 illustrates the localisation of the fused silica atoms before and after the elastic and plastic deformation. The atomic

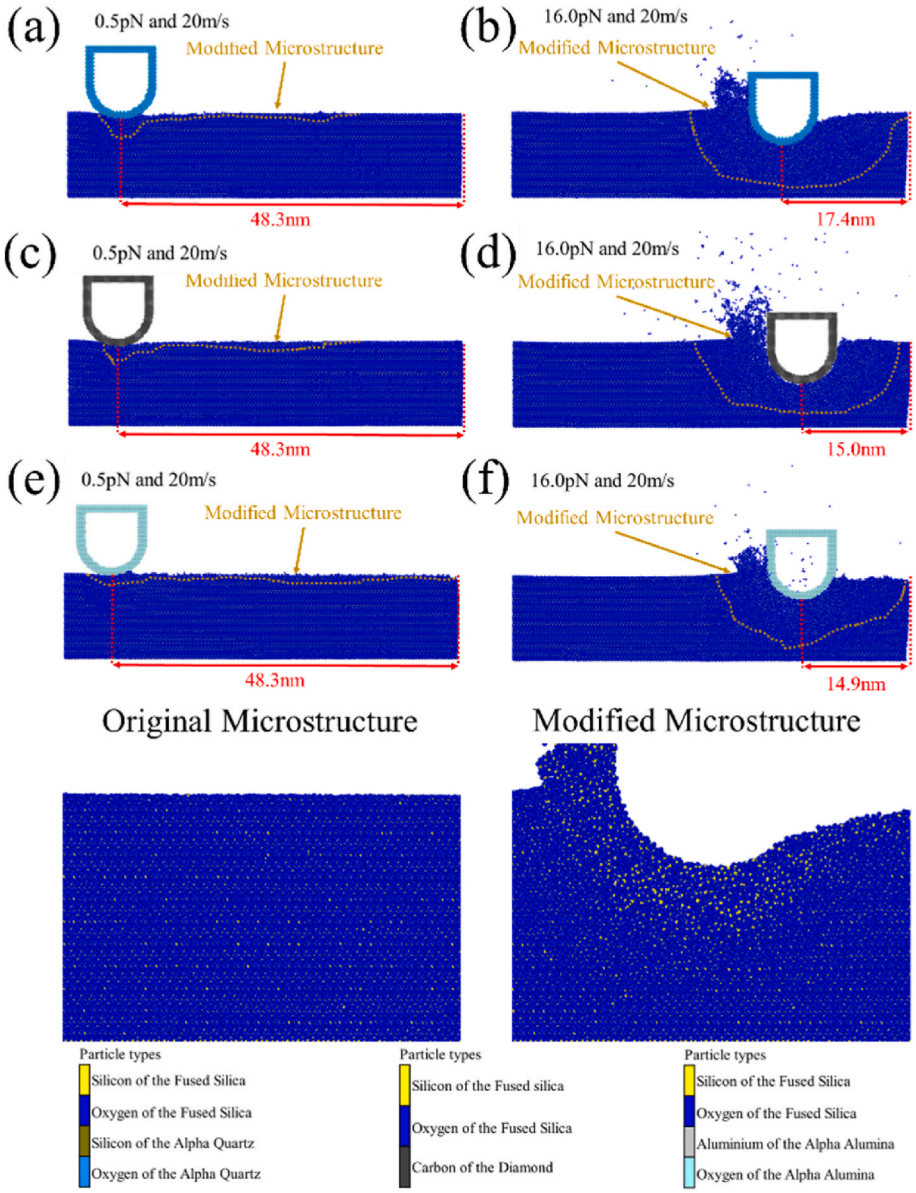

Fig. 8. Ovito transversal pictures of the fused silica polishing simulations with α-quartz (a–b), diamond (c–d) and α-alumina (e–f) at 20 m/s of sliding and grain normal force 0.5 pN on (a), (c) and (e) and 16.0 pN on (b), (d) and (f).

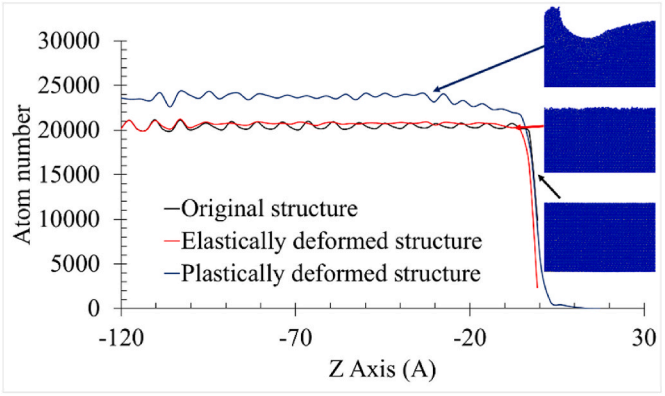

Fig. 9. Graph of the atom number for each position in Z axis for original, elastically and plastically deformed structures.

positions in the elastically deformed structure closely resembled those of the original structure, confirming the shape recovery of the optical glass material for this process. In contrast, for the plastic deformation, a significant atomic displacement was observed, indicating the occurrence of the deformation of the fused silica.

The depth of the microstructure changes increased with the normal load (Grain force). The phenomena are due to the higher normal load on the grain applies higher pressure on the glass materials and generates larger strain diffused into optical glass materials. The strain diffusion depth is increased to the pressure [18,19,31]. Therefore, the higher normal load causes thicker microstructural change zones. The type of the grain influenced less on the modified microstructure, indicating the new microstructure is due to the physical phenomena.

Two types of the polishing process behaviours were observed in the simulations when applying a load force $\leq$ 1.0 pN (Fig. 8(a)–(c), (e)) or $\geq$ 2.0 pN (Fig. 8(b)–(d), (f)). Polishing with lower normal load showed the grain penetration, causing glass deformed that recovered after the grain passing. This indicates that the polishing process is predominated by an elastic deformation. The materials were hardly removed in this case. This phenomenon is attributed to F_G is lower compared with threshold to removal material [62]. The second type of the polishing (normal load $\geq$ 2.0 pN) was characterised by the grain penetration into optical glass material with a chip generation. The grain penetration produced a plastic deformation of the optical glass material. With $F_G \geq$ 2.0 pN, the penetration mechanism occurs continuously during grain sliding and the material removal occurred at the front of the grain. The production of the chip is because the F_G is higher in comparison with the threshold of material removal force. The higher force provokes the displacement of the optical glass materials, being accumulated in the front and lateral of the grain, forming a chip. The chip microstructure was dissimilar to the optical glass material original microstructure. The stress on the fused silica is higher compared with their resistance, which is enough to produce the breaking and deformation of the chemical bonds, creating the new microstructure [18–20,31,33].

It is important to note that the microstructure generated by the dislocations can encourage the material removal by reducing the hardness of the fused silica. The microstructure exhibits significant influence on the mechanical properties of the material, including hardness.

The lateral modification of the optical glass material microstructure can be seen in Fig. 10. Grain stress is produced in 3 dimensions into the optical glass material [18,45], resulting the 3D microstructure modification. In the simulation where the system failed ($\geq$ 2.0 pN), numerous voids or nano-cracks were observed prior to the failure of the system. The stress exerted by the grain on the fused silica induced a new microstructure characterised by the presence of nano-cracks or voids, which are attributed to excessive chemical bond breaking. The excessive microstructural change weakens the chemical bonds, promoting further the bond breaking. The crack formation (instability of the system) occurs when the number of these nano-cracks or avoids becomes substantial [63].

3.3. Tribological phenomena

The behaviour of the friction force (Horizontal force) evolution over time were dissimilar according to the force on grain (Fig. 11.). Friction force of all samples fluctuated during all simulation due to the brittle fracture [21] and dislocation [18,19,64].

The temporal evolution of the friction force exhibited two different behaviours according to the gran force. For grain force $\leq$ 1.0 nN, the behaviour consisted of two steps, while for grain force $\geq$ 2.0 nN, the behaviour comprised three steps. The first behaviour comprised, whereas the second formed of three steps.

The temporal evolution in the first step was the same for both behaviour type. The increase in the friction force characterised the initial step of the simulation. The accumulation of the removed material in front of grain increases the horizontal resistant force. This material hinders the movement of the grain, leading increase in the friction [3,45]. The massing of the material in the grain front is directly proportional to the cut depth and polishing time. The friction force also is directly proportional to grain force on the optical glass material [65].

In the next step, the friction force remained constant over time, as the grain penetration ceased. The grain pressure force is neutralised by opposite normal force exerted by the fused silica, which reminds the penetration depth constant [21]. Notably, this step also was the similar to both behaviour type and constituted last step for the first behaviour ($\leq$ 1.0 nN).

The dramatic reduction in the friction force featured the third and last step for the second behaviour type ($\geq$ 2.0 nN). This step preceded the instability of the system, during which various voids or nano-cracks were generated within the optical glass material. The voids or nano-cracks weaken the optical glass material, thereby reducing the resistance to grain displacement in the material. The maximum friction force was defined as the highest constant horizontal force (second step). Fig. 8 (d) shows the influence of the pressure force and grain type on the maximum friction force. An increase in the grain pressure force results in an increase in the friction force. The force of friction is directly proportional to the normal force acting on the grain [65]. It is noted that the type of grain had influence on the maximum friction, but the mechanism is unclear.

3.4. Material removal rate estimation

The material removal rate (MRR) is one of the primary concerns in polishing process. The schematic drawing of the method employed to calculate MRR can be seen in Fig. 12. MRR can be figured with two different ways, depending on the penetration depth. One estimation way is employed when the cut penetration depth smaller in comparison with the grain radius (Fig. 12(b)), while the other way is utilised for penetration depths are compared to the grain radius (Fig. 12(c)). MRR was estimated using equations (9)–(11) [66], 12, 13, 14 and 15 and the simulation data of the polishing simulations.

$$\begin{cases} MRR = A_A \times V_c \; D_p \leq r_G \\ MRR = A_A \times V_c + \dfrac{A_p \times \Delta X_p}{t} \; D_p > \; r_G \end{cases} \tag{9}$$

$$\begin{cases} A_A = \dfrac{r_G^2}{2} \times \left(\theta^2 + (\cos(\theta))^2 - 1\right) D_p \leq r_G \\ A_A = \dfrac{r_G^2}{2} \times \left(\dfrac{\pi^2}{4} - 1\right) D_p > \; r_G \end{cases} \tag{10}$$

$$\theta = \cos^{-1}\left(1 - \frac{D_p}{r_G}\right) \tag{11}$$

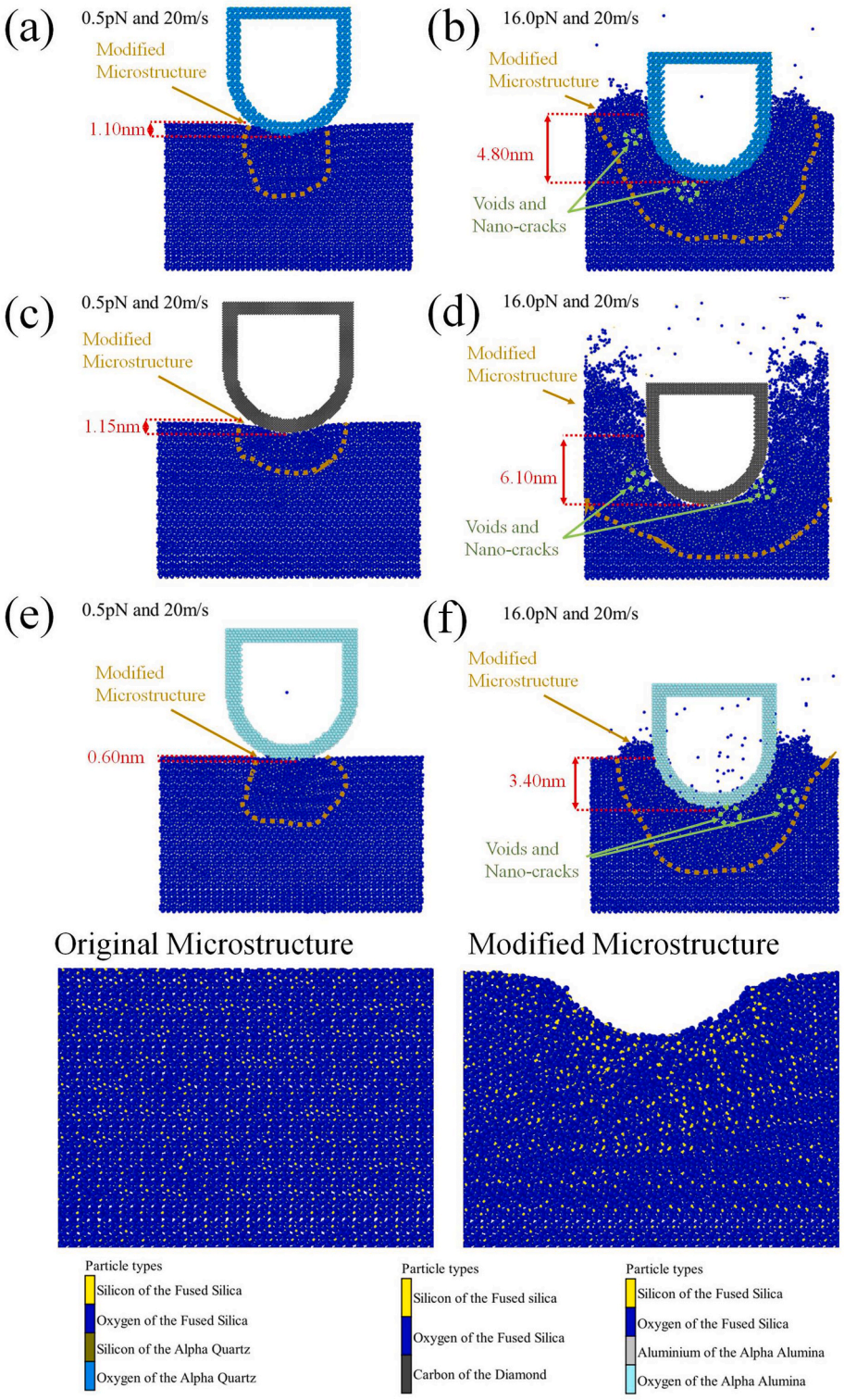

Fig. 10. Ovito cross-section pictures of the fused silica polishing simulations with α-quartz (a–b), diamond (c–d) and α-alumina (e–f) at 20 m/s of sliding and 0.5 pN (a), (c) and (e) and, 16.0 pN (b), (d) and (f) of grain force.

$$A_p = 2 \times r_G \times (D_p - r_G) \tag{12}$$

$$\Delta X_p = V_c \times (t - t_p) \tag{13}$$

$$t_p = \frac{r_G}{R_p} \tag{14}$$

$$R_p = \frac{D_p}{t} \tag{15}$$

Herein, A_A is the arch area of the grain semi-sphere part, t is the total sliding time, A_p is the pylon area of the grain cylindrical part, ΔX_p is the sliding distance after the penetration depth is larger than the grain radius, θ is the penetration angle, D_p is the penetration depth, r_G is the

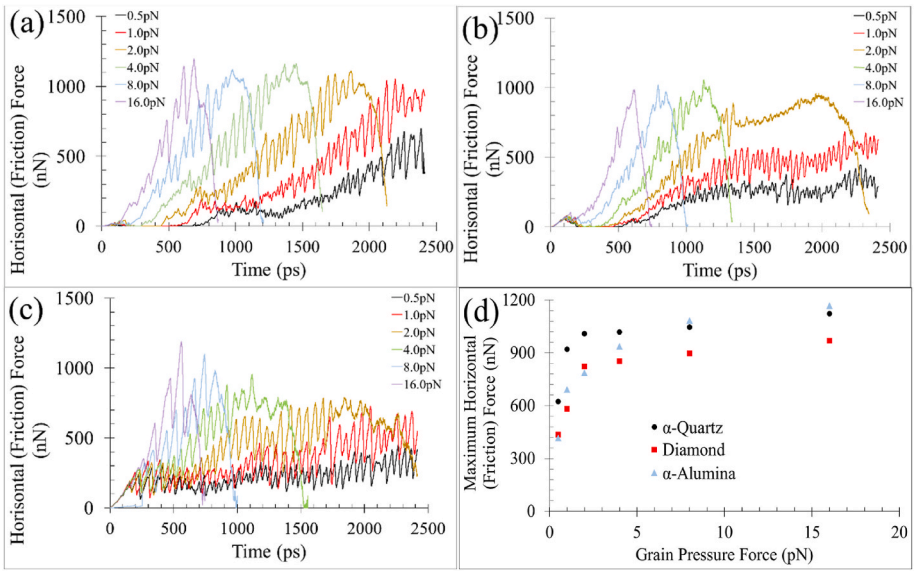

Fig. 11. Graphs of the grain normal force influence on the friction force (horizontal force) for the simulation carried out with α-quartz (a), diamond (b), α-alumina (c) grain and maximum friction force according to the grain pressure force and grain type (d).

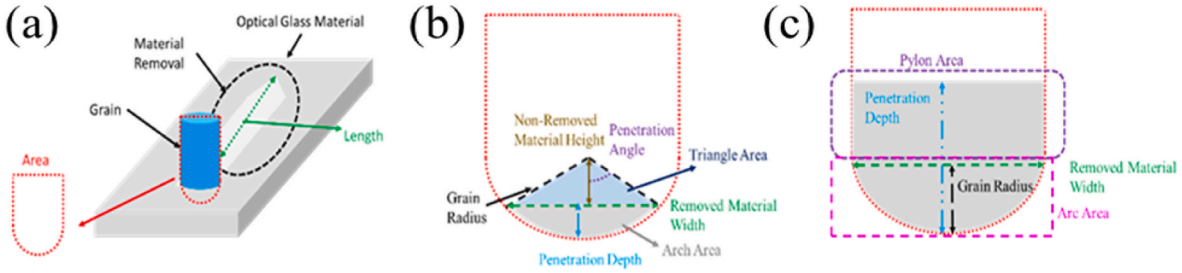

Fig. 12. Schematic drawing of the method used to calculate the material removal (a) when the penetration depth is shorter than grain radius (b) and the penetration depth is longer than grain radius (c).

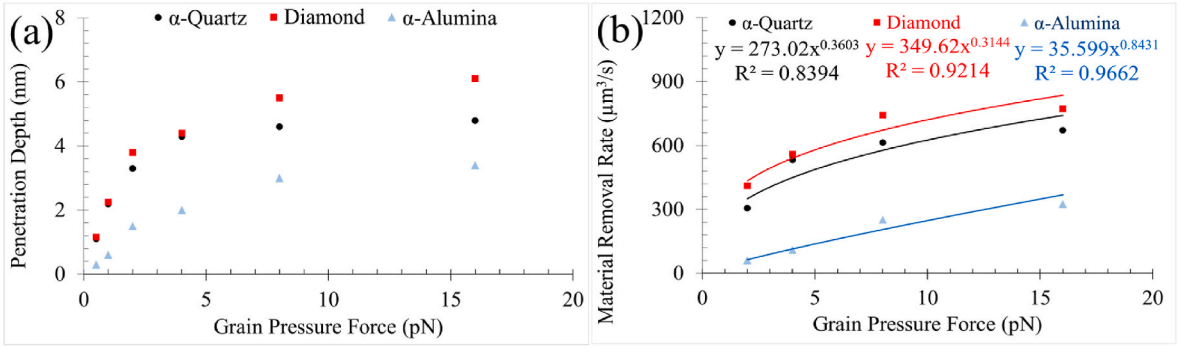

Fig. 13. Graphs of the polishing penetration depth (a), and material removal rate (b) in function to grain pressure force and type.

grain radius, t_p is the time at $D_p = r_G$ and R_p is the penetration depth rate. Note that equations (12)–(14) and, 15 was derived in-house.

The influence of the force on the grain and the type of abrasive powder on polishing parameters (D_p and MRR) can be observed in Fig. 13 and Table 2. The increase in the grain force deepened its penetration into optical glass material during the polishing process (Fig. 10 (a)). The material is penetrated faster owing to structural strength of the optical glass material is rapidly surpassed by the higher normal load of the grain [12,67]. The depth penetration slope with grain pressure force was dissimilar for ≤ 1.0 pN compared to penetration slope for ≥ 2.0 pN because the dissimilar penetration process. For $F_G \leq 1.0$ pN simulations, the penetration mechanism only occurs at end of the grain sliding and most deformation was recoverable. For the simulations at $F_G \geq 2.0$ pN, the penetration mechanism occurs continuously during grain sliding and material removal occurred at the front of the grain. The penetration must begin again in the new position of the grain. The chemical bonds of this new position is less deformed in comparison with the bonds of previous position. The normal load required to penetrate the optical glass material thus is higher compared to the zone with high deformation. This provokes a reduction of the penetration efficiency [22,62].

The penetration or polishing depth varied according to the type of the grain, with the diamond grain exhibited the greatest depth and the

Table 2
Penetration depth and material removal rate of the polishing process according to the grain pressure force and grain type.

Grain pressure force (pN)	α-Quartz		Diamond		α-Alumina	
	Penetration depth (nm)	Material removal rate ($\mu m^3/s$)	Penetration depth (nm)	Material removal rate ($\mu m^3/s$)	Penetration depth (nm)	Material removal rate ($\mu m^3/s$)
0.5	1.10	–	1.15	–	0.30	–
1.0	2.20	–	2.25	–	0.60	–
2.0	3.30	306.74	3.80	411.16	1.50	61.33
4.0	4.30	532.73	4.40	559.18	2.00	109.94
8.0	4.60	614.31	5.50	742.79	3.00	251.96
16.0	4.80	672.45	6.10	773.37	3.40	326.30

α-alumina grain the least. This fact can be attributed to the chemical interactions between the grain and optical glass material, which can impedance the penetration of the grain into the optical glass material. These chemical interactions were absent for the diamond grain due to the high chemical inactivity of the material [68]. In contrast, the chemical interactions are stronger for α-alumina, owing to the greater atomic charge difference between the grain and optical glass material elements. The chemical interaction between both materials was previously observed by Lomic et al. [69]. In the case of the α-quartz grain, the chemical interaction between grain and the optical glass material results in a low modification of the material. This phenomenon is owing to the chemical composition of the α-quartz and fused silica are exactly the same, silicon dioxide [20]. Thus, the chemical element of the system remains constant during the polishing process.

In the most polishing conditions, MRR was figured for the situation of $D_p \leq r_G$. The simulations with diamond grain at 16.0 pN and 8.0 pN were only conditions which $D_p > r_G$. MRR behaviour with respect to the grain pressure force and grain type was similar to the penetration depth behaviour with these parameters (Fig. 10(c)). This indicates that A_A is the most dominant element in MRR, which is defined by D_p. Thus, D_p is the most significant factor in MRR.

F_G influence on MRR for each grain type is represented with equation (16) (α-quartz), (17) (diamond) and (18) (α-alumina), which were made using the power regression of the MRR in function of F_G (Fig. 13(b)).

$$\alpha - \text{quartz } MRR = 273.020 \left(\frac{\mu m^3}{s \times pN}\right) \times F_G^{0.360} \quad (16)$$

$$\text{diamond } MRR = 349.620 \left(\frac{\mu m^3}{s \times pN}\right) \times F_G^{0.314} \quad (17)$$

$$\alpha - \text{alumina } MRR = 35.599 \left(\frac{\mu m^3}{s \times pN}\right) \times F_G^{0.843} \quad (18)$$

The slope of the MRR equations demonstrated an influence with grain type similar to that observed in the grain penetration depth. Thus, the same explanations of the penetration depth behaviour can be applied for the MRR slope. The MRR power behaviour with respect to the grain pressure force was similar to the stress behaviour with this polishing parameter. This fact can suggest that the density of the grain encourages this parameter of the MRR equation.

4. Conclusions

It has been successfully carried out the MD simulation of fused silica polishing processes with various forces (from 0.5 pN to 16 pN) on several grain types (α-quartz, diamond and α-alumina) using Tersoff potential fields. The simulation mimics a single grain motion in the polishing process to represent material removal mechanism. From the simulation, following conclusions are listed.

- The simulations at grain pressure force ≥ 2.0 pN show the glass material failures, leading to a time of system stability. The instability of the system occurs at a lower temperature than the fused silica melting temperature and a high Von Mise stress. This indicates that the crack formation is the cause of the instability of the system. The stability time is shorter at higher grain force due to the increase of the stress on optical glass materials. In opposite to this, the polishing processes at grain pressure force ≤ 1.0 pN are stable during all simulation because the lower stress in the optical glass materials. The stability time is shorter with harder grain than softer one (α-quartz > diamond≈α-alumina).
- Two types of the polishing performance according to the grain force can be found in the simulation. At low grain pressure force (0.5 pN and 1.0 pN), the grain penetrated in the optical glass materials, but no chip formed. The other polishing type is found at medium and high grain pressure force (≥ 2.0 pN) and this is characterised by the chip generation. The material removal thus happens for this kind of polishing. The grain produces a new structure in the chip and the optical glass material zone passed. The deformation and dislocation of the chemical bonds are the cause of this new microstructure.
- The friction force evolution over time can be two dissimilar behaviour types according to the grain pressure force (≤ 1.0 pN and ≥ 2.0 pN). Both evolutions corresponding at the types of polishing processes, the first kind (low grain force) is featured by only penetration of the grain into optical glass material, whilst the second type (high grain force) is characterised by the chip formation and the instability of the system. The increasing of the grain pressure force increases the friction force. The grain type seems to influence in the friction force, but without a clear pattern.
- The cracks are generated at high grain pressure force due to the high kinetic energy promotes their formation. Previous studies have shown that the inclusion of the water in the system could mitigate the crack formation.
- The material removal rate increases with the F_G for all grain kinds. The hardness, density and chemical composition of the grain have influence on the material removal rate. MRR in function to grain force can be presented using power equation. The slope of the equation has a behaviour with the polishing parameters related to the penetration depth whilst the power equation's behaviour with grain pressure force and grain type is related to the Von Mises stress.

This study has provided insight into the polishing mechanisms (low and high grain pressure force), the damages (cracks and microstructural changes), tribological features (without and with chip formation) and MRR modelling for the fused silica polishing under dry condition. The influence of the polishing conditions (grain pressure force and grain type) on these phenomena observed during this process have been thoroughly examined, being the first paper that evaluates the grain chemical composition influence. Thus, the conclusions of this study help to understand the polishing process of the fused silica at nanometre scale in real time and, the influence of the grain chemical composition and force on grain in this process. This will help to define the best condition to carry out the wished polishing, which is a strong topic for various industries. This study does not address the cut velocity, grain shape and, wet influence on the fused silica polishing process, representing a limitation that will be addressed in future research. To simulate the wet

conditions (under water), alternative method for modelling the force field (e.g., Reaxff) will be utilised in future works. This approach is necessary due to the inability of the Tersoff method to simulate hydrogen bonds, which are characteristics of the water.

CRediT authorship contribution statement

Juan I. Ahuir-Torres: Writing – review & editing, Writing – original draft, Visualization, Validation, Resources, Methodology, Investigation, Formal analysis, Data curation, Conceptualization. **Xun Chen:** Writing – review & editing, Writing – original draft, Supervision, Project administration, Methodology, Funding acquisition. **Yasemin Akar:** Writing – review & editing. **Paul A. Bingham:** Writing – review & editing. **Frankie F. Jackson:** Writing – review & editing. **Hongyu Li:** Writing – review & editing. **Luke Mason:** Writing – review & editing. **Rakesh Mishra:** Writing – review & editing. **David D. Walker:** Writing – review & editing. **Guoyu Yu:** Writing – review & editing.

Declaration of interest statement

The authors declare that they have no known competing financial interests or personal relationships that could have appeared to influence the work reported in this paper.

Acknowledgement

This work was supported by the Engineering and Physical Science Research Council EPSRC, UK, Under the skin of polishing - from nano to macro; Grant numbers EP/V029266/1.

References

[1] P. Hartmann, R. Jedamzik, S. Reichel, B. Schreder, Optical glass and glass ceramic historical aspects and recent developments: a Schott view, Appl. Opt. 49 (2010) D157–D176.
[2] R. Rajaramakrishna, J. Kaewkhao, Glass material and their advanced applications, KnE Social Sciences 2019 (2019) kss. v3i18. 4769.
[3] M. Li, X. Guo, R. Zhai, X. Luo, R. Kang, Z. Jin, D. Guo, Study on the subsurface damage mechanism of optical quartz glass during single grain scratching, Ceram. Int. 47 (2021) 7683–7691.
[4] E. Brinksmeier, Y. Mutlugünes, F. Klocke, J. Aurich, P. Shore, H. Ohmori, Ultra-precision grinding, CIRP annals 59 (2010) 652–671.
[5] Y. Zhang, G. Yan, Z. Li, F. Fang, Quality improvement of collimating lens produced by precision glass molding according to performance evaluation, Opt Express 27 (2019) 5033–5047.
[6] A.Y. Yi, A. Jain, Compression molding of aspherical glass lenses–a combined experimental and numerical analysis, J. Am. Ceram. Soc. 88 (2005) 579–586.
[7] T.I. Suratwala, W.A. Steele, L.L. Wong, G.C. Tham, J.F. Destino, P.E. Miller, N. J. Ray, J.A. Menapace, E. Feigenbaum, N. Shen, Subsurface mechanical damage correlations after grinding of various optical materials, Opt. Eng. 58 (2019) 092604.
[8] W. Gu, Z. Yao, K. Li, Evaluation of subsurface crack depth during scratch test for optical glass BK7, Proc. IME C J. Mech. Eng. Sci. 225 (2011) 2767–2774.
[9] X. Han, Y. Hu, S. Yu, Investigation of material removal mechanism of silicon wafer in the chemical mechanical polishing process using molecular dynamics simulation method, Appl. Phys. A 95 (2009) 899–905.
[10] Y. Dong, Q. Li, A. Martini, Molecular dynamics simulation of atomic friction: a review and guide, J. Vac. Sci. Technol. A: Vacuum, Surfaces, and Films 31 (2013) 030801.
[11] S. Goel, X. Luo, A. Agrawal, R.L. Reuben, Diamond machining of silicon: a review of advances in molecular dynamics simulation, Int. J. Mach. Tool Manufact. 88 (2015) 131–164.
[12] V.-T. Nguyen, T.-H. Fang, Molecular dynamics simulation of abrasive characteristics and interfaces in chemical mechanical polishing, Appl. Surf. Sci. 509 (2020) 144676.
[13] Z. Tian, X. Xu, F. Jiang, J. Lu, Q. Luo, J. Lin, Study on nanomechanical properties of 4H-SiC and 6H-SiC by molecular dynamics simulations, Ceram. Int. 45 (2019) 21998–22006.
[14] X. Han, Investigation on the complex interaction between particle and substrate in mechanical polishing of silica glass, Int. J. Adv. Des. Manuf. Technol. 85 (2016) 2567–2575.
[15] S.A. Hollingsworth, R.O. Dror, Molecular dynamics simulation for all, Neuron 99 (2018) 1129–1143.
[16] J. Chen, The development and comparison of molecular dynamics simulation and Monte Carlo simulation. IOP Conference Series: Earth and Environmental Science, IOP Publishing, 2018 012110.
[17] D. Nawrocki, The problems with Monte Carlo simulation, J. Financ. Plann. 14 (2001).
[18] Z. Tian, X. Chen, X. Xu, Molecular dynamics simulation of the material removal in the scratching of 4H-SiC and 6H-SiC substrates, Int. J. Extrem. Manuf. 2 (2020) 045104.
[19] Z. Wu, L. Zhang, S. Yang, Effect of abrasive grain position patterns on the deformation of 6H-silicon carbide subjected to nano-grinding, Int. J. Mech. Sci. 211 (2021) 106779.
[20] X. Guo, C. Zhai, R. Kang, Z. Jin, The mechanical properties of the scratched surface for silica glass by molecular dynamics simulation, J. Non-Cryst. Solids 420 (2015) 1–6.
[21] Q. Luo, J. Lu, Z. Tian, F. Jiang, Controllable material removal behavior of 6H-SiC wafer in nanoscale polishing, Appl. Surf. Sci. 562 (2021) 150219.
[22] Z. Tian, Investigation of Material Removal Mechanism of SiC in Nano-Scale Machining Using Molecular Dynamics Simulation, Liverpool John Moores University, 2021.
[23] Q. Liu, L. Li, Y.-R. Jeng, G. Zhang, C. Shuai, X. Zhu, Effect of interatomic potentials on modeling the nanostructure of amorphous carbon by liquid quenching method, Comput. Mater. Sci. 184 (2020) 109939.
[24] L.-s. Atomic, M.M.P. Simulator, LAMMPS Users Manual, 2003.
[25] B. Wu, Y. Sun, H. Tan, S. Wu, Molecular dynamics investigation of nano-polishing on silicon carbide substrate with rough topography using a rotating diamond abrasive, Mater. Today Commun. 41 (2024) 110744.
[26] A. Stukowski, Visualization and analysis of atomistic simulation data with OVITO–the Open Visualization Tool, Model. Simulat. Mater. Sci. Eng. 18 (2009) 015012.
[27] C. Scherer, Molecular dynamics simulations of silicate and borate glasses and melts: structure, diffusion dynamics and vibrational properties. Mainz, Univ., Diss, 2015, p. 2015.
[28] N.T. Huff, E. Demiralp, T. Cagin, W.A. Goddard III, Factors affecting molecular dynamics simulated vitreous silica structures, J. Non-Cryst. Solids 253 (1999) 133–142.
[29] X. Guo, S. Yuan, X. Wang, Z. Jin, R. Kang, Atomistic mechanisms of chemical mechanical polishing of diamond (1 0 0) in aqueous H_2O_2/pure H_2O: molecular dynamics simulations using reactive force field (ReaxFF), Comput. Mater. Sci. 157 (2019) 99–106.
[30] P. Ranjan, R. Balasubramaniam, V. Jain, Mechanism of material removal during nanofinishing of aluminium in aqueous KOH: a reactive molecular dynamics simulation study, Comput. Mater. Sci. 156 (2019) 35–46.
[31] X. Han, Y. Hu, S. Yu, Investigation of material removal mechanism of silicon wafer in the chemical mechanical polishing process using molecular dynamics simulation method, Appl. Phys. A 95 (2009) 899–905.
[32] Z. Wu, L. Zhang, W. Liu, Structural anisotropy effect on the nanoscratching of monocrystalline 6H-silicon carbide, Wear 476 (2021) 203677.
[33] B. Meng, D. Yuan, S. Xu, Study on strain rate and heat effect on the removal mechanism of SiC during nano-scratching process by molecular dynamics simulation, Int. J. Mech. Sci. 151 (2019) 724–732.
[34] P. Zhang, H. Zhao, C. Shi, L. Zhang, H. Huang, L. Ren, Influence of double-tip scratch and single-tip scratch on nano-scratching process via molecular dynamics simulation, Appl. Surf. Sci. 280 (2013) 751–756.
[35] X. Guo, S. Yuan, J. Huang, C. Chen, R. Kang, Z. Jin, D. Guo, Effects of pressure and slurry on removal mechanism during the chemical mechanical polishing of quartz glass using ReaxFF MD, Appl. Surf. Sci. 505 (2020) 144610.
[36] S.J. Sque, Bulk and transfer doping of diamond, Submitt, Philos. Phys., 1, Univ. Exeter Thesis Degree Dr, 2005, p. 3.
[37] M. Aswad, Residual Stress and Fracture in High Temperature Ceramics, The University of Manchester, United Kingdom, 2012.
[38] S. Munetoh, T. Motooka, K. Moriguchi, A. Shintani, Interatomic potential for Si–O systems using Tersoff parameterization, Comput. Mater. Sci. 39 (2007) 334–339.
[39] S. Goel, X. Luo, R.L. Reuben, Molecular dynamics simulation model for the quantitative assessment of tool wear during single point diamond turning of cubic silicon carbide, Comput. Mater. Sci. 51 (2012) 402–408.
[40] M. Tungare, Y. Shi, N. Tripathi, P. Suvarna, F. Shahedipour-Sandvik, A Tersoff-based interatomic potential for wurtzite AlN, Phys. Status Solidi 208 (2011) 1569–1572.
[41] L. Brugnoli, K. Miyatani, M. Akaji, S. Urata, A. Pedone, New atomistic insights on the chemical mechanical polishing of silica glass with ceria nanoparticles, Langmuir 39 (2023) 5527–5541.
[42] M. Höhnerbach, A.E. Ismail, P. Bientinesi, The vectorization of the tersoff multi-body potential: an exercise in performance portability, SC'16. Proceedings of the International Conference for High Performance Computing, Networking, Storage and Analysis, IEEE, 2016, pp. 69–81.
[43] J. Tersoff, Modeling solid-state chemistry: interatomic potentials for multicomponent systems, Phys. Rev. B 39 (1989) 5566.
[44] P. Gao, X. Duan, J. Guo, J. Wang, Z. Song, L. Cui, X. Meng, X. Liu, W. Zhang, M. Ma, LMFF: efficient and scalable layered materials force field on heterogeneous many-core processors. Proceedings of the International Conference for High Performance Computing, Networking, Storage and Analysis, 2021, pp. 1–14.
[45] H. Dai, F. Zhang, Y. Zhou, Numerical study of three-body diamond abrasive polishing single crystal Si under graphene lubrication by molecular dynamics simulation, Comput. Mater. Sci. 171 (2020) 109214.
[46] X. Han, Study micromechanism of surface planarization in the polishing technology using numerical simulation method, Appl. Surf. Sci. 253 (2007) 6211–6216.
[47] B.J. Garrison, D. Srivastava, Potential energy surfaces for chemical reactions at solid surfaces, Annu. Rev. Phys. Chem. 46 (1995) 373–394.

[48] D. Bullett, Chemical pseudopotential approach to covalent bonding. ii. Bond lengths and bond energies in diamond, silicon and graphite, J. Phys. C Solid State Phys. 8 (1975) 2707.
[49] Y.-R. Luo, J.A. Kerr, Bond Dissociation Energies, CRC Handbook of Chemistry and Physics, vol. 89, 2012, p. 89.
[50] J. O'donoghue, A. Cameron, Friction and temperature in rolling sliding contacts, ASLE TRANSACTIONS 9 (1966) 186–194.
[51] D. Shakhvorostov, K. Pöhlmann, M. Scherge, An energetic approach to friction, wear and temperature, Wear 257 (2004) 124–130.
[52] A. Hapkiewicz, Clarifying chemical bonding, Sci. Teach. 58 (1991) 24.
[53] B. Meng, Y. Zhang, F. Zhang, Material removal mechanism of 6H-SiC studied by nano-scratching with Berkovich indenter, Appl. Phys. A 122 (2016) 1–9.
[54] J.M. Branlund, A.M. Hofmeister, Thermal diffusivity of quartz to 1,000 C: effects of impurities and the α-β phase transition, Phys. Chem. Miner. 34 (2007) 581–595.
[55] T. Anthony, W. Banholzer, J.F. Fleischer, L. Wei, P. Kuo, R. Thomas, R. Pryor, Thermal diffusivity of isotopically enriched C 12 diamond, Phys. Rev. B 42 (1990) 1104.
[56] N. Saheb, U. Hayat, Temperature-dependent thermal properties of spark plasma sintered alumina, Sci. Sinter. 49 (2017).
[57] H.-S. Jang, M.-W. Cho, D.-S. Park, Micro fluidic channel machining on fused silica glass using powder blasting, Sensors 8 (2008) 700–710.
[58] J. Engelder, C. Scholz, The role of asperity indentation and ploughing in rock friction—II: influence of relative hardness and normal load. International Journal of Rock Mechanics and Mining Sciences & Geomechanics Abstracts, Elsevier, 1976, pp. 155–163.
[59] C. Zhang, Molecular Dynamics Simulation of Nanoindentation Test of Corundum ([lowercase Alpha]-Al2O3) on (0001) Surface, University of Florida, 2013.
[60] P.D. Barsanescu, A.M. Comanici, von Mises hypothesis revised, Acta Mech. 228 (2017) 433–446.
[61] E. Estragnat, G. Tang, H. Liang, S. Jahanmir, P. Pei, J. Martin, Experimental investigation on mechanisms of silicon chemical mechanical polishing, J. Electron. Mater. 33 (2004) 334–339.
[62] Q. Jia, W. He, D. Hua, Q. Zhou, Y. Du, Y. Ren, Z. Lu, H. Wang, F. Zhou, J. Wang, Effects of structure relaxation and surface oxidation on nanoscopic wear behaviors of metallic glass, Acta Mater. 232 (2022) 117934.
[63] W.-L. Zhu, A. Beaucamp, Compliant grinding and polishing: a review, Int. J. Mach. Tool Manufact. 158 (2020) 103634.
[64] Q. Pei, C. Lu, H. Lee, Y. Zhang, Study of materials deformation in nanometric cutting by large-scale molecular dynamics simulations, Nanoscale Res. Lett. 4 (2009) 444–451.
[65] Z. Ye, P. Egberts, G.H. Han, A.C. Johnson, R.W. Carpick, A. Martini, Load-dependent friction hysteresis on graphene, ACS Nano 10 (2016) 5161–5168.
[66] P. Degond, L. Pareschi, G. Russo, Modeling and Computational Methods for Kinetic Equations, Springer Science & Business Media, 2004.
[67] A.A. Tseng, C.-F.J. Kuo, S. Jou, S. Nishimura, J.-i. Shirakashi, Scratch direction and threshold force in nanoscale scratching using atomic force microscopes, Appl. Surf. Sci. 257 (2011) 9243–9250.
[68] M.Z. Hossain, T. Kubo, T. Aruga, N. Takagi, T. Tsuno, N. Fujimori, M. Nishijima, Surface phonons, electronic structure and chemical reactivity of diamond (100)(2× 1) surface, Jpn. J. Appl. Phys. 38 (1999) 6659.
[69] G.A. Lomić, E.E. Kiss, Subtle interactions in silica-alumina mixtures, React. Kinet. Catal. Lett. 95 (2008) 61–69.